IEEE Access
Multidisciplinary | Rapid Review | Open Access Journal

Received 22 August 2022, accepted 26 September 2022, date of publication 3 October 2022, date of current version 10 October 2022.

Digital Object Identifier 10.1109/ACCESS.2022.3211320

RESEARCH ARTICLE

A *X* −/*Ka*-Band Linearly Polarized Low Profile Shared-Aperture Antenna Array for Satellite Applications

YONG YANG[1], YONG-LING BAN[1], (Member, IEEE), QIANG SUN[1], AND CHOW-YEN-DESMOND SIM[2], (Senior Member, IEEE)

[1]School of Electronic Science and Engineering, University of Electronic Science and Technology of China, Chengdu 611731, China
[2]Department of Electrical Engineering, Feng Chia University, Taichung 47025, Taiwan

Corresponding author: Yong-Ling Ban (byl@uestc.edu.cn)

This work was supported in part by the National Natural Science Foundation of China under Grant 61971098 and Grant U19A2055, in part by the National Key Research and Development Project under Grant 2020YFB1805003, and in part by the Fund of Science and Technology on Electromagnetic Scattering Laboratory under Grant 61424090410.

ABSTRACT An *X* −/*Ka*-band shared aperture scanning antenna array for satellite applications is proposed. The Ka-band antenna array consists of 8 × 8 antenna elements in a triangular grid, while the X-band antenna array consists of 4 × 4 antenna elements in a rectangular grid. Notably, the antenna elements of Ka band array and X-band array are planar microstrip dipole antennas to avoid structural overlap and reduce mutual coupling. Besides, the *X*-band antenna elements and *Ka*-band antenna elements are interlaced to share the same aperture. Compared with the recently released dual band shared aperture antenna array, the profile of the proposed antenna array is only 0.05 times the air wavelength. The frequency ratio (f_{high}/f_{low}) of the proposed antenna array is 3.1, and the antenna number ratio (N_{Ka}/N_X) of the antenna array is 4. These two parameters are close, which can improve the aperture utilization of the array. The measurement results show that the scanning angles of the antenna array at 10GHz and 30GHz are 38° and 30°, respectively.

INDEX TERMS Millimeter wave, shared-aperture antenna array, scanning antenna array, dipole antenna.

I. INTRODUCTION

In recent years, low profile dual band shared aperture antenna arrays have gradually become a research hotspot. One reason is that antenna arrays working in multiple bands can provide more and richer communication services and functions. Another reason is that the shared aperture layout can improve the aperture utilization of multi band antenna arrays. In addition, low profile design of the antenna arrays can be more easily compatible with the structure of the platform. Therefore, the research on low profile dual band shared aperture scanning antenna array is very valuable.

Dual band shared aperture scanning antenna array is mainly realized in the following ways. The first way is that antenna elements of different frequency bands shares one structure [6], [7], [8]. Among them, in [6] and [7], the profiles of the shared aperture antenna arrays are 0.08 wavelength and 0.07 wavelength respectively. However, their low-frequency antennas are single antenna elements, which cannot provide beam scanning function. Although the antenna array in [8] can realize a scanning angle up to 40°, its antenna elements are three-dimensional structure with high profiles. It is clear to see that the shared aperture antenna array realized by sharing one structure is often difficult to meet the requirements of low profile and beam scanning at the same time.

The second way is that the elements of different frequency bands are interlaced with each other [9], [10], [11]. Among them, in [9] and [10], the scanning angle of the antenna array reaches 50° and 30°, respectively, but due to the use of 6-layer dielectric substrates, their profiles reach 0.3 wavelength and 0.5 wavelength, respectively. In [11], the antenna array only uses three-layer dielectric substrates, so that the

The associate editor coordinating the review of this manuscript and approving it for publication was Hussein Attia.

This work is licensed under a Creative Commons Attribution 4.0 License. For more information, see https://creativecommons.org/licenses/by/4.0/

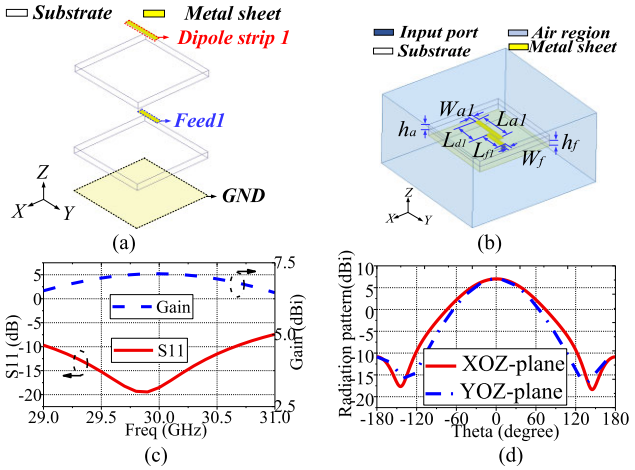

FIGURE 1. Configuration and simulated results of the Ka-band antenna element. (a) Separated view. (b) aligned view with parameters (dimension: $L_{a1} = 3.1$mm, $L_{f1} = 4$mm, $L_{d1} = 1.55$mm, $W_f = 0.4$mm, $W_{a1} = 0.6$mm, $h_f = 0.508$mm, $h_a = 0.508$mm). (c) S11. (d) patterns at 30 GHz.

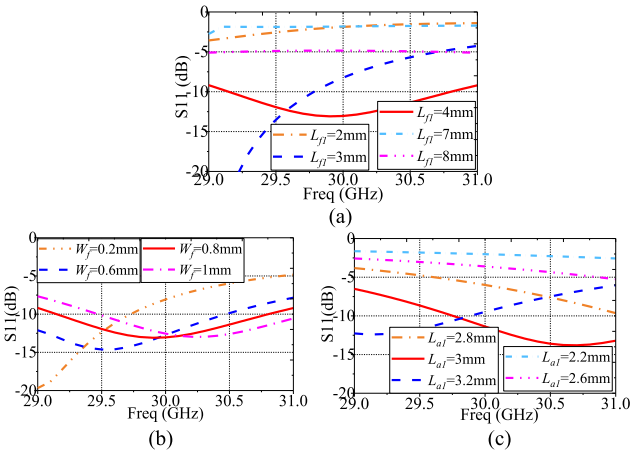

FIGURE 2. Parameters sweep of the Ka-band antenna element. (a) S11 with different values of L_{f1}. (b) S11 with different values of W_f. (c) S11 with different values of L_{a1}.

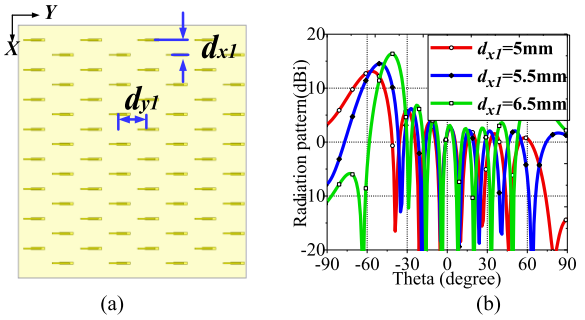

FIGURE 3. Configuration and results of the *Ka*-band antenna array. (a) configuration. (b) simulated beams of different d_{x1} with a PPD = 150°.

profile is only 0.04 wavelength, but the beam scanning performance is not mentioned.

The third way is that the elements of one frequency band are stacked to the antenna elements of another frequency band. In [12], the antenna array can realize beam scanning, and its profile is only 0.04 wavelength. However, the antenna number ratio of the shared aperture antenna arrays is much larger than the frequency ratio, which diminishes the aperture utilization of the antenna array.

According to the reference [11], [12], it is clear to see that the requirements of low profile and beam scanning of dual band shared aperture antenna array can be realized by reducing the number of layers of dielectric substrates and adopting the way of interlacing elements or stacking elements. Thus, This paper proposes a *X*-/*Ka*-band shared-aperture scanning antenna array(now denoted as proposed array) realized by the way of interlacing elements. In addition, the proposed antenna array only contains three layers of dielectric substrates, which diminishes the profile. The *X*-band antenna array of the proposed antenna array is composed of 4 × 4 elements with an operating frequency of 9.75–10.25 GHz, and the *Ka*-band antenna array is composed of 8 × 8 elements with an operating frequency of 29.5-30.5 GHz. Because the mutual coupling between arrays will affect the performance of antenna array, it needs to be suppressed [13], [14], [15], [16]. In this paper, the planar microstrip dipoles with small size are used as the array elements of the two working bands, which reduces the mutual coupling and improves the isolation between the two band. Different from [12], the proposed antenna array has an antenna number ratio of 4, which is close to the frequency ratio of 3. Thus, the aperture utilization of the proposed antenna array is up to 75%. In addition, the scanning angles of the proposed antenna array are up to 38° in the *X*-band and 30° in the *Ka*-band, respectively.

II. DERIVATION OF THE *X*-/*Ka*-BAND SHARED-APERTURE ANTENNA ARRAY

A. DESIGN OF THE Ka- BAND ANTENNA ARRAY

The structure and simulated results of the *Ka*-band antenna element are summarized in Fig. 1. As shown in Figs. 1(a) and Figs. 1(b), the structure of the *Ka*-band antenna element is composed of three metal layers and two dielectric substrates [17]. The layout of the *Ka*-band antenna element is as follows: the dipole strip 1 act as the radiation part is located in the top metal layer, the feed1 act as feed part is located in the middle metal layer, and the bottom metal layer is the reference ground (GND). In addition, the main parameters-of the *Ka*-band antenna element are summarized in Fig. 1(b). Notably, the two layers of dielectric are chosen to be 0.508 mm to reduce the feed loss and expand the bandwidth of the antenna element.

The simulated results of the *Ka*-band antenna element are summarized in Fig. 1(c) and (d). The *Ka*-band antenna element can achieve S11s less than −10-dB and gains gain larger than 6 dBi in the range from 29-30.5 GHz, as shown in Fig.1(c). In addition, the radiation pattern of the *Ka*-band antenna element at 30 GHz is shown in Fig. 1(d), where the 3-dB gain beamwidth of the E-plane (XOZ plane) and

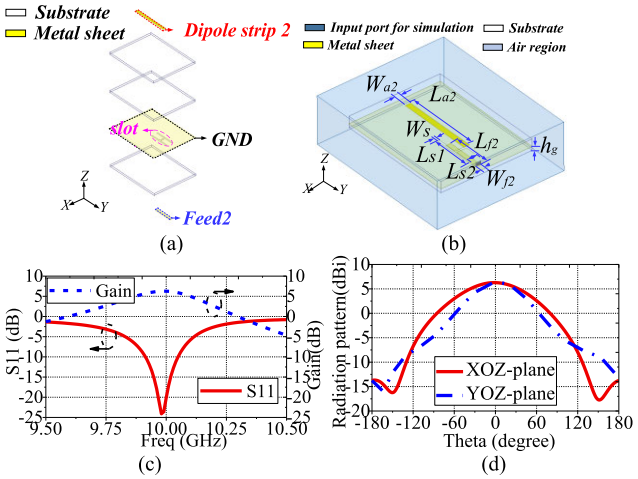

FIGURE 4. Configuration and simulated results of the *X*-band antenna element. (a) Separated view. (b) Aligned view with parameters(dimension: L_{a2} = 10.2mm, W_{a2} = 1.1mm, W_s = 0.3mm, L_{s1} = 5.4mm, L_{s2} = 1.4mm, L_{f2} = 6mm, W_{f2} = 0.7mm, h_g = 0.508mm).(c) S11.(d) Patterns at 10GHz.

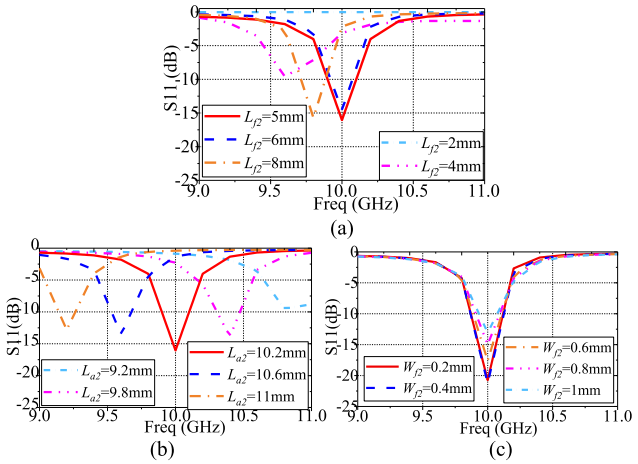

FIGURE 5. Parameters sweep of the *X*-band antenna element. (a) S11 with different values of L_{f2}. (b) S11 with different values of W_{f2}. (c) S11 with different values of L_{a2}.

H-plane (YOZ plane) can reach 80°, and the front to back ratio (F/B ratio) is larger than 15 dB.

Fig. 2 shows the influence of the main size parameters of the *Ka*-band antenna element on the reflection coefficient S11. The selected size parameters are the length L_{f1} of the feed 1, the width W_f of the feed 1, and the length L_{a1} of the antenna element. As shown in Fig.2, all of L_{a1}, W_f and L_{a1} have significant impacts on the resonance frequency of the S11. Specifically, when L_{f1} = 4mm, W_f = 0.6-1mm and L_{a1} = 3.1mm, the S11 of the *Ka*-band antenna element has a minimized value at the center frequency of 30GHz.

Thus, a *Ka*-band antenna array based on the above *Ka*-band antenna element is designed. To reserve sufficient space for the subsequent *X*-band antenna array, it is necessary to appropriately widen the spacing between two adjacent *Ka*-band antenna elements. However, in the traditional rectangular grid plane array, when the antenna array element spacing

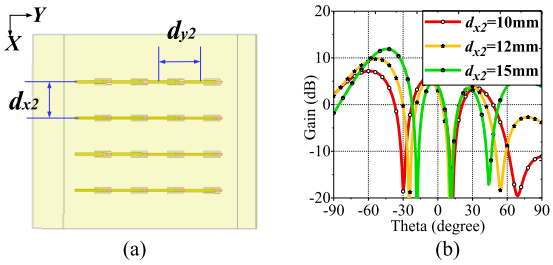

FIGURE 6. Configuration and results of the *X*-band antenna array. (a) configuration. (b) simulated beams of different d_{x2} with a PPD = 150°.

exceeds 0.5 wavelength, the grating lobe levels of scanning beams will be greater than 10dB. Therefore, the *Ka*-band antenna array adopts a triangular grid layout to ensure that the grating lobe level of the scanning beam will not deteriorate when the array element spacing exceeds 0.5 wavelength [18].

The structure and simulated results of the proposed *Ka*-band antenna array are shown in Fig. 3, where the *Ka*-band antenna array is composed of 8 × 8 antenna elements. Here, the parameters d_{x1} and d_{y1} are the distances between two adjacent antenna elements in the X-direction and Y-direction, respectively. Taking the case of beam scanning in E-plane (XOZ plane) as an example, the scanning beams with different d_{x1} has been analyzed, where d_{x1} varies from 5–6.5 mm and the port phase difference (PPD) is set to 150°. As depicted in Fig. 3(b), when d_{x1} = 5 mm, the beams of the *Ka*-band antenna array can achieve a maximum scanning angle of 50°. Besides, when d_{x1} = 6.5 mm, the maximum beams scanning angle of the *Ka*-band antenna array is 45°, but the grating lobe has deteriorated to −7 dB at this time. Thus, d_{x1} is set to 6mm to ensure that the scanning angle of the beam can reach 30°.

B. DESIGN OF THE X- BAND ANTENNA ARRAY

The structure and simulated results of the *X*-band antenna element are shown in Figs. 4(a)-(d). Here, the antenna element is composed of three metal layers and two dielectric substrates, as shown in Figs. 4(a) and (b). The layout of the X-band antenna element is as follows: dipole strip 2 act as the radiation part is located in the upper metal layer. GND with a loaded H-shaped slot is located in the middle metal layer, and feed 2 is located in the bottom layer. The size parameters of the *X*-band antenna element are shown in Fig. 4(b). The simulated results of the *X*-band antenna element are shown in Figs. 4(c) and (d). The *X*-band antenna element has achieved S11s less than −10-dB and gains larger than 3dBi in the frequency range from 9.9 to 10.1 GHz. In addition, the radiation pattern of the *X*-band antenna element at 10 GHz has been shown in Fig.4(d), where the 3-dB beam width in the E plane (XOZ plane) is 80°, and the beam width in the H plane (YOZ plane) is 50°. Besides, the F/B ratio of the beam is better than 15dB.

Similarly, Fig. 5 shows the influence of the main size parameters of the *X*-band antenna element on the reflection

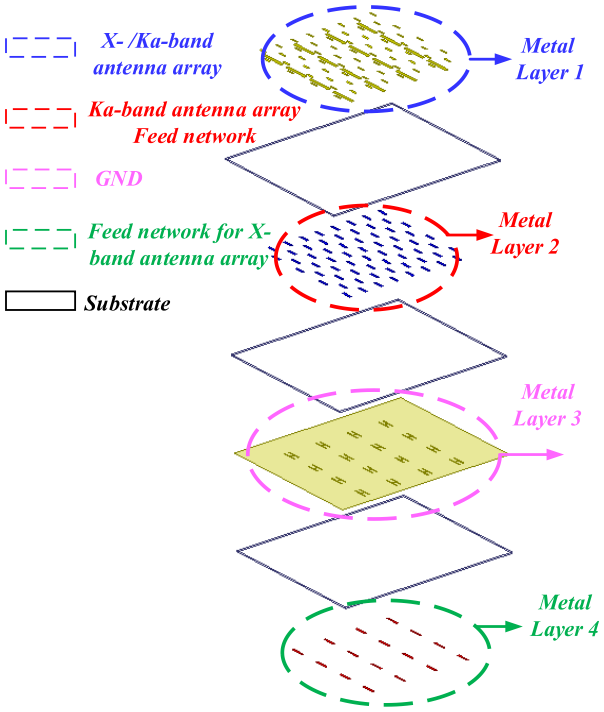

FIGURE 7. Configuration of the proposed *X*−/*Ka*-band shared-aperture antenna array.

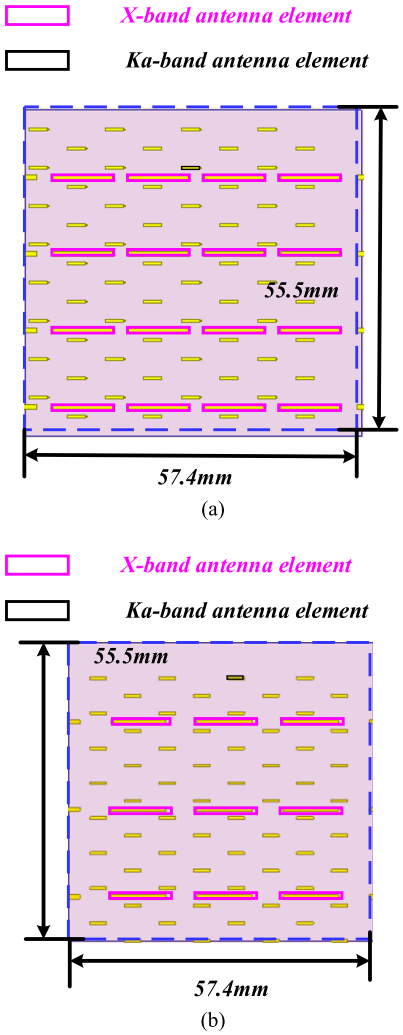

FIGURE 8. Configuration of the *X*−/*Ka*-band shared-aperture antenna array with different value of *Nka*/*Nx*. (a) *Nka*/*Nx* = 4. (b) *Nka*/*Nx* = 7.

coefficient S11. The selected size parameters are the length L_{f2} of the feed 2, the length W_{f2} of the feed 2, and the length L_{a2} of the antenna element. As shown in Fig.2, both L_{f2} and L_{a2} significantly affect the resonant frequency of S11, and W_{f2} only affects the value at the resonant point of S11. Specifically, when $L_{f2} = 4$mm, $W_{f2} = 0.8$mm and $L_{a2} = 3.1$mm, the S11 of *X*-band antenna element has the minimized value at the center frequency of 10GHz.

Similar to the *Ka*-band antenna array, the *X*-band antenna array can be designed based on the *X*-band antenna element. Fig. 6(a) shows the structure of the *X*-band antenna array, which is a rectangular planar array composed of 4×4 elements, and d_{x2} and d_{y2} are the spacing between *X*-band antenna elements. Fig. 6(b) shows the simulated scanning beams of the *X*-band antenna array when d_{x2} varies from 10–15 mm, where PPD = 150°. Here, when $d_{x2} = 12$ mm ($0.4\lambda_x$), the maximum scanning angle of the beams can reach 55°. Notably, when $d_{x2} = 15$ mm ($0.55\lambda_x$), the scanning angle is less than 45° and the grating lobe level is larger than -10dB. Thus, d_{x2} is set to 12mm to ensure that the scanning angle of the beam can reach 38° and the grating lobe level less than −10dB.

C. PROPOSED X-/Ka- BAND SHARED APERTURE SCANNING ANTENNA ARRAY

The proposed *X*-/*Ka*- band shared aperture scanning antenna array is a composition of the *Ka*-band and *X*-band antenna array analyzed above. Its structure is shown in Fig. 7, and it is composed of four metal layers and three dielectric layers. The layout of the metal layers is as follows; Firstly, the *X*-band antenna elements and the *Ka*-band antenna elements are located on the metal sheet 1 and interlaced with each other. Secondly, to ensure the *X*-band antenna element does not overlap with the *Ka*-band antenna structure, distance parameters d_{x2}, d_{y2}, d_{x1} and d_{y1} should satisfy the following relationship that $d_{x2} = 2d_{x1}$ and $d_{y2} = 2d_{y1}$. Thirdly, the feed networks of *Ka*-band antenna elements are located on the metal sheet 2. Forthly, the metal layer 3 is the GND of the whole shared aperture antenna array. Finally, the feed networks of the *X*-band antenna array are located at the metal layer 4.

The aforementioned layout for the antenna element is considered as follows. First, as shown in Fig. 7, both *X*-band and *Ka*-band use dipole stripes as antenna elements have a smaller area than the traditional square microstrip patch antenna. This layout can avoid structure overlapping of antenna elements when *X*-band antenna elements and *Ka*-band antenna elements are interlaced to each other.

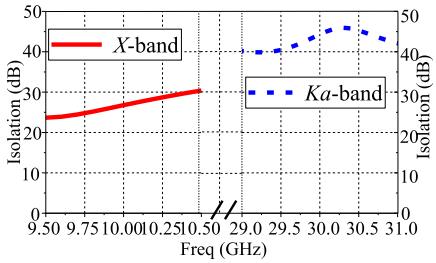

FIGURE 9. Simulated isolations between *X*-band input port and *Ka*-band input port.

Secondly, the *Ka*-band antenna element spacing parameter d_{x1} is set to 6mm (0.6 wavelength), which can ensure that the scanning angle of the *Ka*-band antenna array can reach to 30°. Notably, setting the *X*-band antenna element spacing parameter d_{x2} to 12 mm (0.5 wavelength) can ensure that the scanning angle of the *X*-band antenna array can reach to 38°. The *Ka*-band antenna array adopts a triangular grid array so that when the distance between adjacent antenna elements reaches 0.6 wavelength, the grating lobe levels of the beams are still less than −10 dB. Since the grating lobe level of the *X*-band antenna array within the scanning range is less than −10 dB, a rectangular grid array is adopted. Finally, the *X*-band and *Ka*-band antenna arrays are all located on the uppermost layer of the entire antenna array, so that the pattern distortion of the antenna arrays in these two frequency bands can be avoided.

Then, the antenna number ratio of the proposed antenna array is discussed. antenna number ratio is defined as the ratio between the number of *Ka*-band antenna elements and that of *X*-band antenna elements when the Ka-band array is and the *X*-band array share similar area. The antenna number ratio of the shared aperture antenna array has an impact on the aperture utilization η, where $\eta = (f_{high}/f_{low})/(N_{high}/N_{low})$. To illustrate this point, this paper shows the structures of the proposed shared aperture antenna array and the aperture utilizations when the antenna number ratio is different, as shown in Fig. 8.

As shown in Fig. 8 (a), when the number of *Ka*-band antenna elements is 64 and the number of *X*-band antenna elements is 16, the antenna number ratio is 4. Thus, the aperture utilization of the proposed *X*-/*Ka*-band shared aperture antenna array equals $3/4 = 75\%$. Similarly, as shown in Fig. 8 (b), when the number of *Ka*-band antenna elements is 64 and the number of *X*-band antenna elements is 9, the antenna number ratio is 7. Thus, the aperture utilization of the proposed *X*-/*Ka*-band shared aperture antenna array equals $3/7 = 42\%$. It is clear to see that the closer the frequency ratio is to the frequency ratio, the higher the aperture utilization. That's why the scheme with the antenna number ratio of 4 is adopted in this paper.

The reasons for this layout of the feed networks of the two frequency bands are as follows. Firstly, to maximize the working bandwidth of the antenna array, the proposed

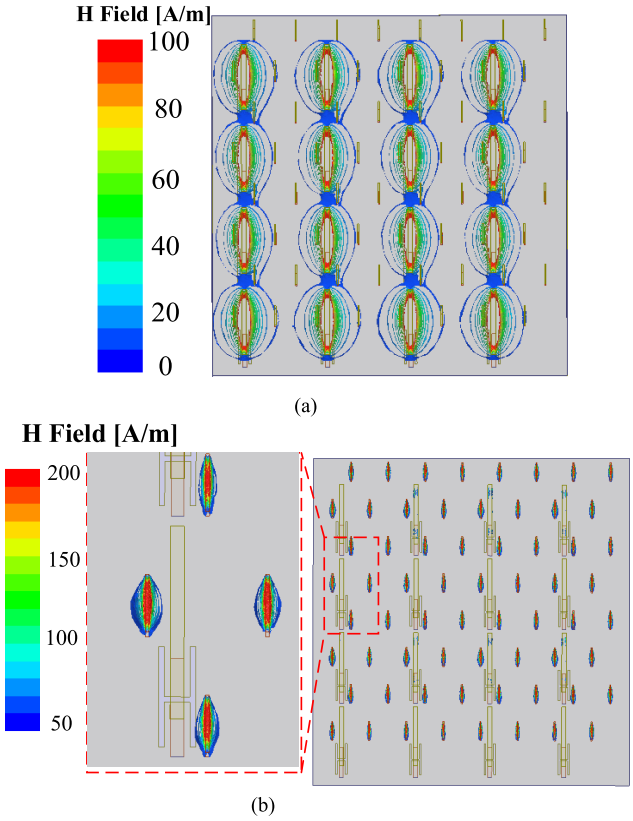

FIGURE 10. H-field distribution. (a) 10 GHz. (b) 30 GHz.

antenna array adopts a parallel feed network topology. However, the feed network of parallel feed tends to have a large area, so the feed networks of the *X*-band antenna array and feed networks of the *Ka*-band antenna array cannot be placed on the same metal layer. Second, since the distance between the *Ka*-band antenna elements is very close, it is necessary to ensure that the width of the feed lines of *Ka*-band network are sufficiently narrow to bypass the *X*-band antenna elements. Besides, if a microstrip line with a narrow line width is adopting the aperture-coupled method through the slot on the ground, the back-lobe level of the antenna array will increase. Therefore, the feed network of the *Ka*-band antenna array is put above the GND, and that of the *X*-band antenna array is put below the GND.

To verify that the proposed array can operate as desired, the isolation performance between the *X*-band antenna array and the *Ka*-band antenna array is analyzed. As shown in Fig. 9, isolations between the *X*-band antenna input port and the *Ka*-band antenna input port are larger than 23dB in the *X*-band and larger than 35dB in the *Ka*-band, respectively. Fig. 10 shows the dielectric layer magnetic-field (H-field) distributions of the proposed array. As depicted in Fig. 10(a), when the *X*-band antenna array is excited at 10 GHz, its H-field amplitude reaches 100A/m, while the H-field of the *Ka*-band antenna array is only less than 20 A/m. This shows that only a small amount of energy is coupled to the Ka band

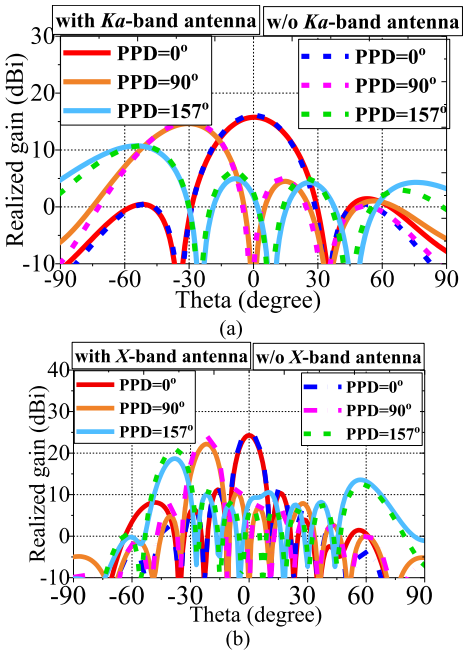

FIGURE 11. Simulated beams between the proposed *X*−/*Ka*-band shared-aperture antenna array and the *X*-band antenna array at. (a) 10 GHz. (b) 30 GHz.

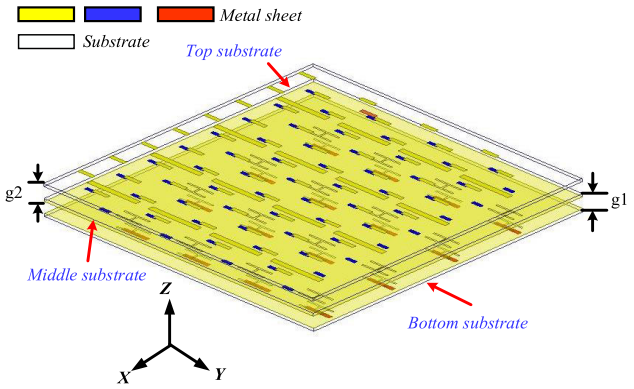

FIGURE 12. Configuration of the proposed *X*−/*Ka*-band shared-aperture antenna array with air gap.

antenna array when the X-band antenna array works alone. Because the coupling energy is very small, Ka band antenna array cannot work, so the electromagnetic field isolation performance of X-band array and Ka band array is good. Similarly, the *X*-band antenna array is slightly coupled when the *Ka*-band antenna array is excited at 30 GHz, as depicted in Fig. 10(b). Therefore, Fig. 10 has validated that the electromagnetic field isolations between *X*-band antenna array and *Ka*-band antenna array of the proposed array are also very good.

The radiation patterns of the proposed array with different PPD (0°, 90°, and 157°) in 10 GHz and 30 GHz are also studied and plotted in Fig. 11. As depicted in Fig. 11(a), the *X*-band beams of proposed array are similar to those of the single *X*-band antenna array. As depicted in Fig. 11(b), the beams of proposed array in the *Ka*-band are also well

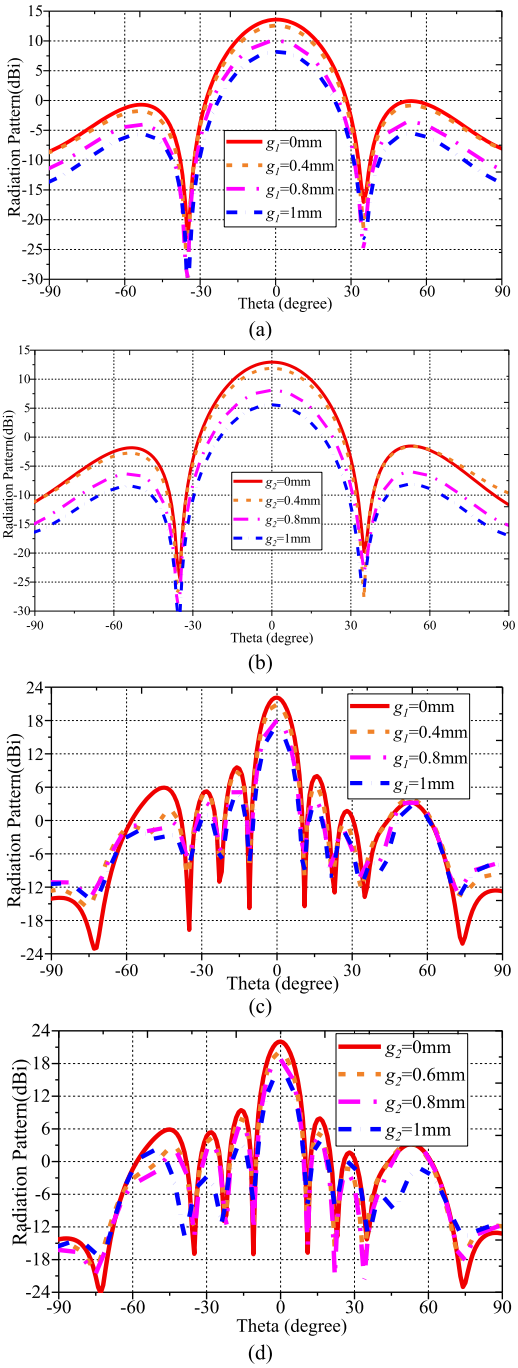

FIGURE 13. Simulated beams. (a) g_1 with different value at 10GHz. (b) g_2 with different value at 10GHz. (c) g_1 with different value at 30GHz. (d) g_2 with different value at 30GHz.

matched with those of the single *Ka*-band antenna array at 30GHz. Here, the beam scanning ranges of (0°, −55°) and (0°, −45°) are achieved at the *X*-/*Ka*-band, respectively.

Then, the influence of the air gap between the dielectric layers on the antenna array is analyzed. Different from the single-layer antenna array, the air gaps of multi-layer antenna array structure will have influences on the antenna performance, which needs to be discussed. The simulated model is shown in the Fig.12, which is similar to the structure of

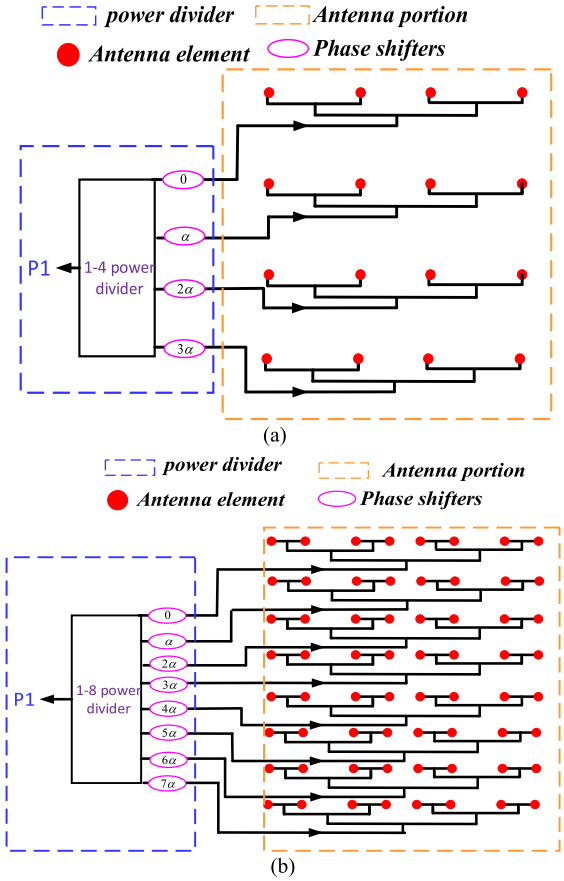

FIGURE 14. Schematic diagram of the feed networks. (a) *X*-band. (b) *Ka*-band.

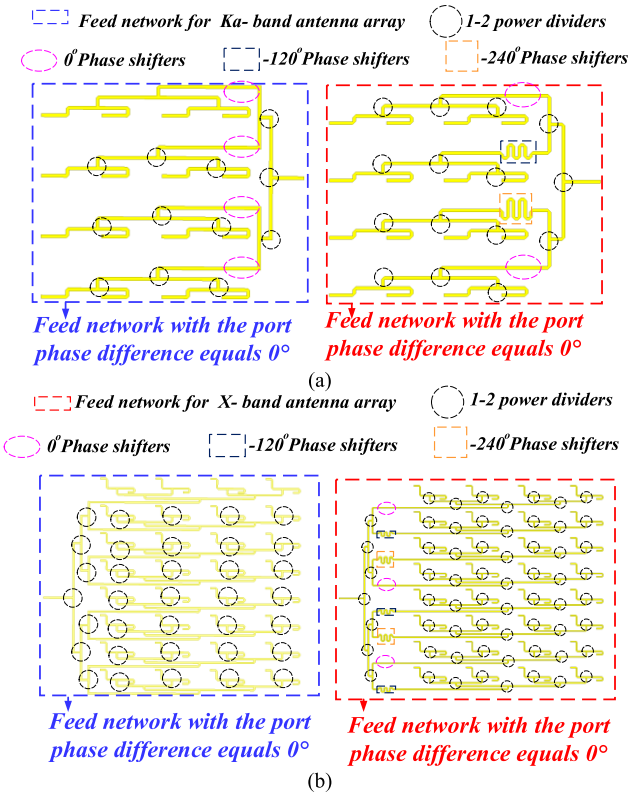

FIGURE 15. Configuration of the feed networks. (a) feed networks for *X*-band antenna-array. (b) feed networks for *Ka*-band antenna-array.

antenna array in Fig.7, except that there are two air gaps between each layer of dielectric substrates. It should be noted that the thickness of the air gap between the lowest substrate and the middle substrate is named as g_1, and the thickness of the air layer between the middle substrate and the uppermost substrate is named as g_2. Then, Fig.13 shows the patterns of antenna array when parameters g_1 and g_2 take different values.

As depicted in Fig.13, the increase of the thickness g_1 and g_2 will reduce the gain of the proposed antenna array whether at 10GHz or 30GHz. In addition, the increase of g_1 and g_2 will also improve the profile of the antenna array. Therefore, in the proposed antenna array, each layer of dielectric substrates was stacked without air gap ($g_1 = g_2 = 0$mm) to avoid the decline of beam gain and reduce the profile.

D. DESIGN OF THE FEED NETWORK

In order to verify the proposed *X*-/*Ka*-band shared aperture antenna array, beams with two scanning angles are selected in *X*-band and *Ka*-band, respectively [19], [20]. Among them, the selected *X*-band scanning angles are 0° and 38°, respectively. And the selected *Ka*-band scanning angles are 0° and 30°, respectively. It should be noted that the scanning planes of the above beams are XOZ planes. Then, two groups of *X*-band feed networks and two groups of *Ka*-band feed networks need to be designed according to the above scanning angle. The schematic diagrams of *X*-band and *Ka*-band feed networks are shown in Fig.14, which are composed of power dividers and phase shifters. The phase differences between adjacent ports of the phase shifters of the feed network are determined in this way. For the *X*-band feed network, the scanning angle of the selected beam is 0° and 38°, so the phase differences of the output ports of the two groups of feed networks can be calculated as 0° and 120°, respectively. Similarly, the phase differences between the adjacent ports of the two groups of *Ka*-band feed networks are 0° and 120°, respectively. The structures of the designed feed networks realized by microstrip lines are shown in Fig. 15.

Then, the feed networks are connected with the proposed antenna arrays to form two *X*-/*Ka*-band shared aperture scanning antenna arrays, called Type-A and Type-B. For Type-A, the phase differences between adjacent ports of *X*-band feed network and *Ka*-band feed network are 0°, so the scanning angles of *X*-band beam and *Ka*-band beam are 0°.

For Type B, the phase difference between the adjacent ports of *X*-band feed network and *Ka*-band feed network is 120°, so the scanning angles of *X*-band beam and *Ka*-band beam are 38° and 30°, respectively. It should be noted that in Type B, the scanning angle of *X*-band beam is different from that of *Ka*-band beam, which is caused by the difference between the number of antenna elements of *X*-band antenna array and *Ka*-band antenna array. In addition, the simulated models of Type-A and Type-B are shown in Fig.16.

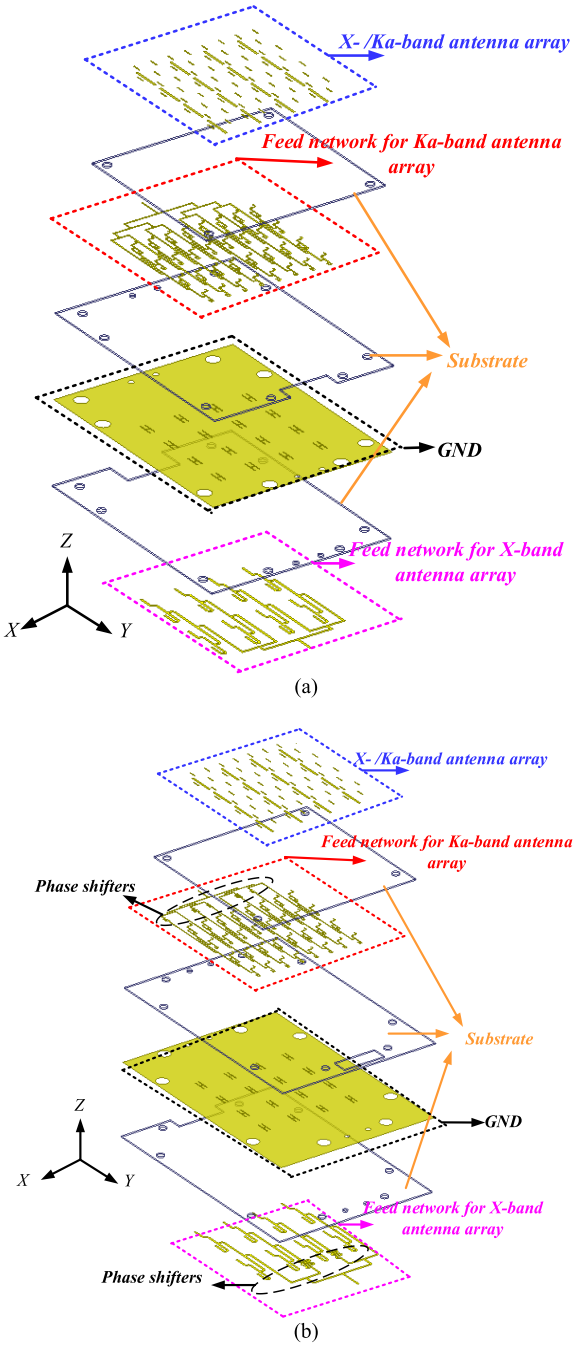

FIGURE 16. Configuration of fabricated *X*−/*Ka*- band shared-aperture antenna array for simulation. (a) Type-A (b) Type-B.

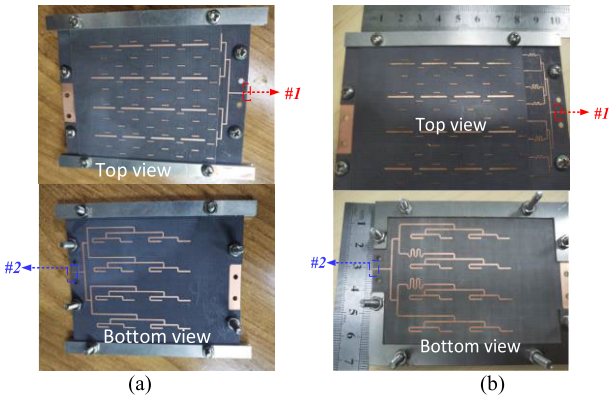

FIGURE 17. Picture of the fabricated *X*−/*Ka*- band shared-aperture antenna array. (a) Fabricated Type-A. (b) Fabricated Type-B.

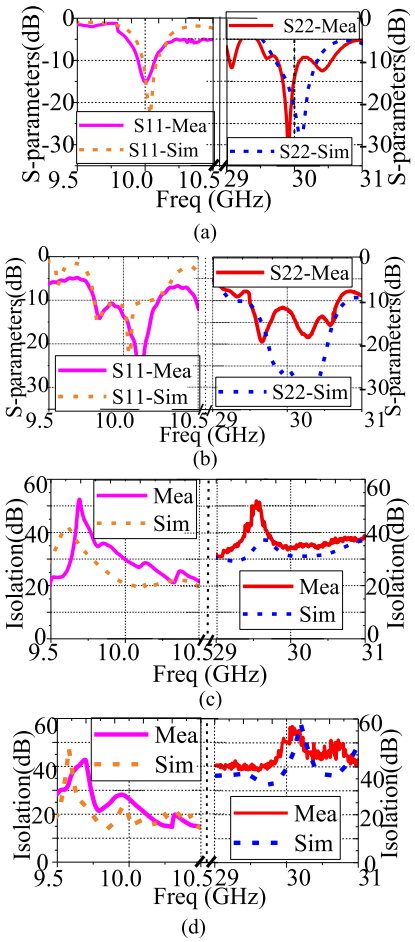

FIGURE 18. Measured and simulated S-parameters. (a) S_{11} and S_{22} of Type-A. (b) S_{11} and S_{22} of Type-B. (c) Isolation of Type-A. (d) Isolation of Type-B.

III. FABRICATION AND MEASUREMENT

The picture of the fabricated Type-A and Type-B are shown in Figs. 17. Besides, a microwave anechoic chamber (NSI-2000) is used to measure the Type-A and Type-B.

The reflection coefficient curves of *X*-band and *Ka*-band for Type-A and Type-B are shown in Figs. 18(a) and Figs. 18(b), respectively. Here, the simulated S11s and S22s of Type-A and Type-B are well-validated with the measured ones, respectively, except that measured S22s have unexpected harmonic modes, which may be due to slight fabrication error such as air gaps during assembly and the reflection of the coax connector. Nevertheless, in the range of 9.9-10.2 GHz, all S11s of Type-A and Type-B are less than −10dB. In addition, in the range of 29.5-to 30.6 GHz, all S22s of Type-A and Type-B are less than −10dB. By further observing the isolation level plotted in Figs. 18(c) and Figs. 18(d), Type-A exhibits an isolation greater than 20 dB in 9.5-10.5 GHz, whereas its corresponding isolation in Type-B was only >13 dB, which is due to the loading of additional

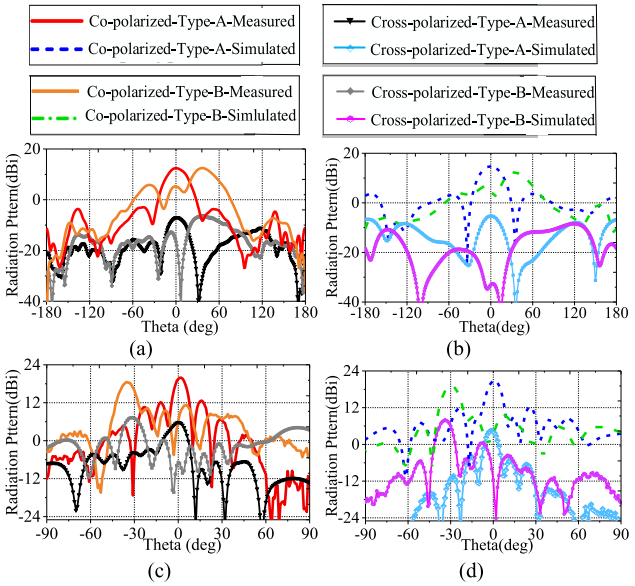

FIGURE 19. Measured and simulated beam at. (a) Measured radiation patterns at 10 GHz. (b) Simulated radiation patterns at 10 GHz. (c) Measured radiation patterns at 30 GHz. (d) Simulated radiation patterns at 30 GHz.

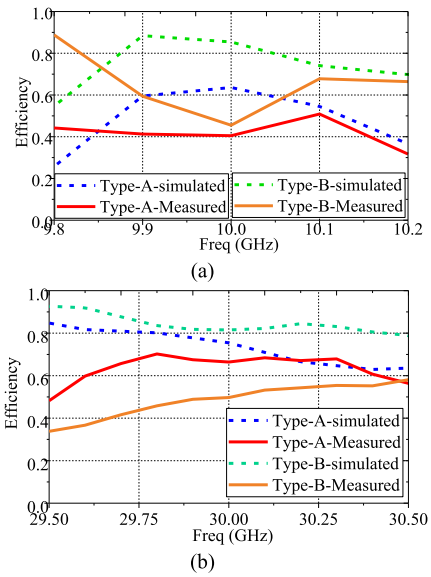

FIGURE 20. Measured efficiency. (a) X-band. (b) Ka-band.

phase shifters in close proximity with the H-shaped slot of *X*-band antenna elements. Notably, very desirable isolation levels of >30 dB were measured across the *Ka*-band of the two prototypes.

The measured and simulated radiation patterns of the two prototypes at 10 GHz and 30 GHz are plotted in Fig. 19(a) - Figs. 19(d), respectively, and the measured results are well-validated with the simulated ones. At 10 GHz, the scanning angles of Type-A and Type-B are approximately 0° and 38°, respectively. The measured maximum gain (MMG) of Type-A reaches 12.6 dBi, and that of Type B reaches 12.8 dBi. At 30 GHz, the scanning angles of Type-A and Type-B are approximately 0° and −30°, respectively. Here,

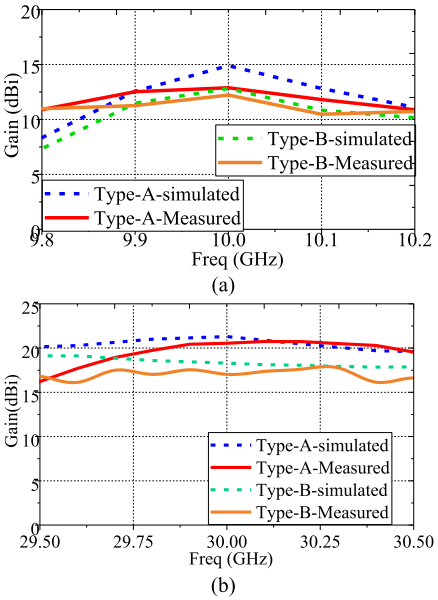

FIGURE 21. Measured gains. (a) *X*-band. (b) *Ka*-band.

the MMG of Type-A reaches approximately 20.1 dBi, and the MMG of Type B reaches approximately 17.5 dBi. The maximum gain difference between *X*-band and *Ka*-band are 7.5 dB and 5.7 dB for Type-A and Type-B, respectively.

As depicted in Fig.20, the maximum efficiencies of the proposed antenna array are 45% and 65% in *X*- band and *Ka*-band, respectively. In addition, the gains of the proposed antenna array in the operating frequency band is shown in Fig.21. It can be seen that in the *X*-band, the gains of the proposed antenna array type-A and type-B are in the range of 11.5dBi-12.6dBi and in the range of 11dBi-12.8dBi, respectively. In addition, in the *Ka*-band, the gains of the proposed antenna array type-A and type-B are in the range of 16.5dBi-20.1dBi and in the range of 16.4dBi-17.5dBi, respectively. Notably, the discrepancy between the measured and simulated results is mainly caused by the alignment errors and fabrication errors.

IV. COMPARISON

The comparison between the proposed *X*-/*Ka*-band shared aperture scanning antenna array and other dual band arrays is shown in Table 1. In [6] and [7], the low-frequency antenna of the shared aperture antenna arrays are single elements, and the beam scanning characteristics are not mentioned. The shared aperture antenna array in [8], [9], and [10] have the disadvantage of high profile. In [11], the beam scanning performance of shared aperture antenna array is not analyzed. The antenna number ratio of the shared aperture antenna array in [12] is greater than the frequency ratio, which reduces the aperture utilization of the array. Different from the above antenna array, the proposed *X*-/*Ka*-band shared aperture scanning antenna array can meet the requirements of low profile and beam scanning in the operation band at the same time. Besides, the antenna number ratio is close to the frequency ratio, which improves the aperture utilization.

TABLE 1. Performances comparison between the proposed work and other references.

Ref.	Freq (GHz)	f_{high}/f_{low} ratio	N_{high}/N_{low} ratio	Antenna-geometry	array	Minimum Profile	Max θ_0	Maximum Gain(dBi)	Efficiency (%)
[1]	5.3/9.6	1.81	NM	Patch/Slot	Yes/Yes	NM	0°/0°	NM/NM	NM/NM
[6]	3.6/25.8	8	64	Patch/Slot	No/Yes	0.08λ	0°/0°	10.88/22.4	65.3/43
[7]	3.5/60	17	144	Slot/Patch	No/Yes	0.07λ	0°	7.3/24	NM/57
[8]	20/30	1.5	1	Dipole/Open waveguide	Yes/Yes	NM	40°/40°	13.2/17.2	76.03/74.4
[9]	20/30	1.5	2	Patch / Patch	Yes/Yes	0.3λ	50°/50°	NM	NM
[10]	1.25/3.6/10	1.2/8	1.6/10.5	Dipole/ Patch/ Patch	Yes/Yes/Yes	NM	30°/30°/30°	13.2/18.6/21.79	NM
[11]	9.6/14.8/34.5	1.5/3.7	4/1	Patch/Dipole/ Patch	Yes/Yes/Yes	0.04λ	0°/0°/0°	13.8/18.1/19.2	85/82/80
[12]	3.1/9.1	2.9	11	Metasurafce/patch	Yes/Yes	0.04λ	50°/50°	NM	NM
This work	10/30	3.1	4	planar	Yes/Yes	0.05λ	40°/30°	12.8/20.1	45/65

NM: not mentioned.

V. CONCLUSION

An *X*−/*Ka*-band shared-aperture scanning antenna array has been proposed for the SAR in satellite applications. The *Ka*-band antenna array is a triangular grid planar array made up of 8 × 8 antenna elements and the *X*-band antenna array is a square grid planar array made up of 4 × 4 antenna elements. The antenna elements of the *X*-band array and the *Ka*-band array are microstrip dipole antenna. By interlacing the *Ka*-band antenna elements and the *X*-band antenna elements with each other, the proposed shared-aperture antenna array can be obtained. Due to the use of compact antenna elements and the way of interlacing the antenna elements of the two frequency bands, the isolation between the *X*-band antenna elements and *Ka*-band antenna elements are higher than 30dB at the operation band of 10GHz and 30GHz. Notably, the proposed antenna array achieves an antenna number ratio (N_{Ka}/N_X) of 4, which is close to the f_{high}/f_{low} equals 3.1. Thus, the aperture availability is up to 75%. In addition, the overall structure profile of the proposed antenna array is only $0.05\lambda_X$, where λ_X is the air wavelength at 10GHz. The measured results show that a scanning angle of up to 38°, an efficiency of 45%, and a maximum gain of 12.8 dBi can be achieved in *X*-band. Besides, a scanning angle of up to 30°, an efficiency of 65%, and a maximum gain of 20.1dBi can be achieved in *Ka*-band.

REFERENCES

[1] R. Pokuls, J. Uher, and D. M. Pozar, "Dual-frequency and dual polarization microstrip antennas for SAR applications," *IEEE Trans. Antennas Propag.*, vol. 46, no. 9, pp. 1289–1296, Sep. 1998.

[2] W. Imbriale, S. Gao, and L. Boccia, Eds., *Space Antenna Hand Book*. Hoboken, NJ, USA: Wiley, 2012.

[3] L. L. Shafai, W. A. Chamma, M. Barakat, P. C. Strickland, and G. Seguin, "Dual-band dual-polarized perforated microstrip antennas for SAR applications," *IEEE Trans. Antennas Propag.*, vol. 48, no. 1, pp. 58–66, Jan. 2000.

[4] M. Alibakhshikenari, E. M. Ali, M. Soruri, M. Dalarsson, M. Naser-Moghadasi, B. S. Virdee, C. Stefanovic, A. Pietrenko-Dabrowska, S. Koziel, S. Szczepanski, and E. Limiti, "A comprehensive survey on antennas on-chip based on metamaterial, metasurface, and substrate integrated waveguide principles for millimeter-waves and terahertz integrated circuits and systems," *IEEE Access*, vol. 10, pp. 3668–3692, 2022.

[5] M. Alibakhshikenari, B. Virdee, L. Azpilicueta, M. Naser-Moghadasi, M. O. Akinsolu, C. H. See, B. Liu, R. Abd-Alhameed, F. Falcone, I. Huynen, T. Denidni, and E. Limiti, "A comprehensive survey of metamaterial transmission-line based antennas: Design, challenges, and applications," *IEEE Access*, vol. 8, pp. 144778–144808, 2020.

[6] T. Li and Z. N. Chen, "Metasurface-based shared-aperture 5G S-/K-band antenna using characteristic mode analysis," *IEEE Trans. Antennas Propag.*, vol. 66, no. 12, pp. 6742–6750, Dec. 2018.

[7] J. F. Zhang, Y. J. Cheng, Y. R. Ding, and C. X. Bai, "A dual-band shared-aperture antenna with large frequency ratio, high aperture reuse efficiency, and high channel isolation," *IEEE Trans. Antennas Propag.*, vol. 67, no. 2, pp. 853–860, Feb. 2019.

[8] Y. R. Ding and Y. J. Cheng, "Ku/Ka dual-band dual-polarized shared-aperture beam-scanning antenna array with high isolation," *IEEE Trans. Antennas Propag.*, vol. 67, no. 4, pp. 2413–2422, Apr. 2019.

[9] A. I. Sandhu, E. Arnieri, G. Amendola, L. Boccia, E. Meniconi, and V. Ziegler, "Radiating elements for shared aperture Tx/Rx phased arrays at K/Ka band," *IEEE Trans. Antennas Propag.*, vol. 64, no. 6, pp. 2270–2282, Jun. 2016.

[10] S.-S. Zhong, Z. Sun, L.-B. Kong, C. Gao, W. Wang, and M.-P. Jin, "Tri-band dual-polarization shared-aperture microstrip array for SAR applications," *IEEE Trans. Antennas Propag.*, vol. 60, no. 9, pp. 4157–4165, Sep. 2012.

[11] C.-X. Mao, S. Gao, Q. Luo, T. Rommel, and Q.-X. Chu, "Low-cost X/Ku/Ka-band dual-polarized array with shared aperture," *IEEE Trans. Antennas Propag.*, vol. 65, no. 7, pp. 3520–3527, Jul. 2017.

[12] C. X. Bai, Y. J. Cheng, Y. R. Ding, and J. F. Zhang, "A metamaterial-based $S-/X$ -band shared-aperture phased-array antenna with wide beam scanning coverage," *IEEE Trans. Antennas Propag.*, vol. 68, no. 6, pp. 4283–4292, Jun. 2020.

[13] A. A. Althuwayb, "Low-interacted multiple antenna systems based on metasurface-inspired isolation approach for MIMO applications," *Arabian J. Sci. Eng.*, vol. 47, no. 3, pp. 2629–2638, Mar. 2022.

[14] M. Alibakhshikenari, F. Babaeian, B. S. Virdee, S. Aïssa, L. Azpilicueta, C. H. See, A. A. Althuwayb, I. Huynen, R. A. Abd-Alhameed, F. Falcone, and E. Limiti, "A comprehensive survey on various decoupling mechanisms with focus on metamaterial and metasurface principles applicable to SAR and MIMO antenna systems," *IEEE Access*, vol. 8, pp. 192965–193004, 2020.

[15] M. Alibakhshikenari, M. Khalily, B. S. Virdee, C. H. See, R. A. Abd-Alhameed, and E. Limiti, "Mutual-coupling isolation using embedded metamaterial EM bandgap decoupling slab for densely packed array antennas," *IEEE Access*, vol. 7, pp. 51827–51840, 2019.
[16] M. Alibakhshikenari, M. Khalily, B. S. Virdee, C. H. See, R. Abd-Alhameed, and E. Limiti, "Mutual coupling suppression between two closely placed microstrip patches using EM-bandgap metamaterial fractal loading," *IEEE Access*, vol. 7, pp. 23606–23614, 2019.
[17] H. Oltman and D. Huebner, "Electromagnetically coupled microstrip dipoles," *IEEE Trans. Antennas Propag.*, vol. AP-29, no. 1, pp. 151–157, Jan. 1981.
[18] E. Sharp, "A triangular arrangement of planar-array elements that reduces the number needed," *IRE Trans. Antennas Propag.*, vol. 9, no. 2, pp. 126–129, Mar. 1961.
[19] J.-W. Lian, H. Zhu, Y.-L. Ban, D. K. Karmokar, and Y. J. Guo, "Uniplanar high-gain 2-D scanning leaky-wave multibeam array antenna at fixed frequency," *IEEE Trans. Antennas Propag.*, vol. 68, no. 7, pp. 5257–5268, Jul. 2020.
[20] R. F. Ma, Z. H. Jiang, Y. Zhang, X. Y. Wu, T. Yue, W. Hong, and D. H. Werner, "Theory, design, and verification of dual-circularly polarized dual-beam arrays with independent control of polarization: A generalization of sequential rotation arrays," *IEEE Trans. Antennas Propag.*, vol. 69, no. 3, pp. 1369–1382, Mar. 2021.
[21] Q. Luo, S. Gao, W. Li, M. Sobhy, I. Bakaimi, C. H. K. de Groot, B. Hayden, I. Reaney, and X. Yang, "Multibeam dual-circularly polarized reflectarray for connected and autonomous vehicles," *IEEE Trans. Veh. Technol.*, vol. 68, no. 4, pp. 3574–3585, Apr. 2019.
[22] J. Zhu, Y. Yang, S. Li, S. Liao, and Q. Xue, "Dual-band dual circularly polarized antenna array using FSS-integrated polarization rotation AMC ground for vehicle satellite communications," *IEEE Trans. Veh. Technol.*, vol. 68, no. 11, pp. 10742–10751, Nov. 2019.
[23] H. B. Wang and Y. J. Cheng, "Single-layer dual-band linear-to-circular polarization converter with wide axial ratio bandwidth and different polarization modes," *IEEE Trans. Antennas Propag.*, vol. 67, no. 6, pp. 4296–4301, Jun. 2019.

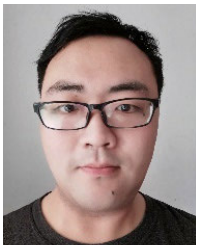

YONG YANG was born in Gansu, China, in 1994. He received the B.S. degree from the University of Electronic Science and Technology of China (UESTC), Chengdu, China, in 2016, where he is currently pursuing the Ph.D. degree. His current research interests include phased antenna array and circularly polarized antenna.

YONG-LING BAN (Member, IEEE) was born in Henan, China. He received the B.S. degree in mathematics from Shandong University, in 2000, the M.S. degree in electromagnetics from Peking University, in 2003, and the Ph.D. degree in microwave engineering from the University of Electronic Science and Technology of China (UESTC), in 2006. In July 2006, he joined the Xi'an Mechanical and Electric Information Institute, as a Microwave Engineer. He then joined Huawei Technologies Company Ltd., Shenzhen, China, as a RF Antenna Design Engineer and then as a Senior Design Engineer. At Huawei, he designed and implemented various terminal antennas for 15 data card and mobile phone products customized from leading telecommunication industries like Vodafone. Since September 2010, he has been an Associate Professor of microwave engineering with the UESTC. He holds 20 granted and pending Chinese and overseas patents. His research interests include wideband small antennas for 4G/5G handset devices, MIMO antenna, and millimeter wave antenna array. He is the author of over 60 refereed journals and conference papers on these topics.

QIANG SUN was born in Henan, China, in September 1994. He received the B.S. degree in communication engineering from the North China University of Water Resources and Electric Power, Zhengzhou, China, in 2017. He is currently pursuing the Ph.D. degree in electromagnetic field and microwave technology with the University of Electronic Science and Technology of China (UESTC), Chengdu, China. His current research interests include millimeter wave antennas and arrays.

CHOW-YEN-DESMOND SIM (Senior Member, IEEE) was born in Singapore, in 1971. He received the B.Sc. degree from the Engineering Department, University of Leicester, U.K., in 1998, and the Ph.D. degree from the Radio System Group, Engineering Department, University of Leicester, in 2003. From 2003 to 2007, he was an Assistant Professor with the Department of Computer and Communication Engineering, Chienkuo Technology University, Changhua, Taiwan. In 2007, he joined the Department of Electrical Engineering, Feng Chia University (FCU), Taichung, Taiwan, as an Associate Professor, where he became a Full Professor, in 2012, and a Distinguish Professor, in 2017. He has served as an Executive Officer of Master's Program with the College of Information and Electrical Engineering (Industrial Research and Development) and the Director of Intelligent IoT Industrial Ph.D. Program, from August 2015 to July 2018. He has Co-Founded the Antennas and Microwave Circuits Innovation Research Center, Feng Chia University, and served as the Director, from 2016 to 2019. He has also served as the Head of the Department of Electrical Engineering, Feng Chia University, from August 2018 and July 2021. He has authored or coauthored over 180 SCI papers. His current research interests include antenna design, VHF/UHF tropospheric propagation, and RFID applications. He is a fellow of the Institute of Engineering and Technology (FIET), a Senior Member of the IEEE Antennas and Propagation Society, and a Life Member of the IAET. He was a recipient of the IEEE Antennas and Propagation Society Outstanding Reviewer Award (IEEE TRANSACTION ANTENNAS AND PROPAGATION) for eight consecutive years, from 2014 to 2021. He has also received the Outstanding Associate Editor Award from the IEEE ANTENNAS WIRELESS AND PROPAGATION LETTERS, in July 2018. He has served as a TPC member for many international conferences, the TPC Sub-Committee Chair (Antenna) for the ISAP 2014 and PIERS 2017/2019, an Advisory Committee for InCAP 2018/2019 and ICoICCS 2021, the TPC Chair for the APCAP 2016 and iWEM 2019/2020, the Track Chair for ICCC 2022, and the Chapter Chair of the IEEE AP-Society, Taipei Chapter, from January 2016 to December 2017. He was invited as the Workshop/Tutorial Speaker in APEMC 2015, iAIM 2017, and InCAP 2018, and the Invited Speaker of TDAT 2015, iWAT 2018, APCAP 2018, ISAP 2019, InCAP 2019, ISRAST 2020, ISAP 2020, NEAST 2020, URSI GASS 2021, iWEM 2021, WAMS 2022, and APCAP 2022. He was also the Keynote Speaker of IEEE SOLI 2018 and the General Co-Chair of ISAP 2021. He is the Founding Chapter Chair of the IEEE Council of RFID, Taipei Chapter, from October 2017 to December 2020. He has served as an Associate Editor for IEEE ACCESS, from August 2016 to January 2021. He is serving as an Associate Editor for the IEEE ANTENNAS AND WIRELESS PROPAGATION LETTERS (AWPL), IEEE JOURNAL OF RADIO FREQUENCY IDENTIFICATION (RFID), and *International Journal of RF and Microwave Computer-Aided Engineering* (Wiley). Since October 2016, he has been serving as a Technical Consultant for the Securitag Assembly Group (SAG), which is one of the largest RFID tag manufacturers in Taiwan. He has also been a Consultant of Avary (the largest PCB manufacturer in mainland China), since August 2018.